Journal of Electronic Materials (2022) 51:1–7
https://doi.org/10.1007/s11664-021-09274-z

BRIEF COMMUNICATION

Reduction Behavior of Surface Oxide on Submicron Copper Particles for Pressureless Sintering Under Reducing Atmosphere

Tomoki Matsuda[1] · Daiki Yamagiwa[1] · Hideki Furusawa[2] · Kenji Sato[2] · Hisashi Yashiro[3] · Keigo Nagao[3] · Jungeun Kim[3] · Tomokazu Sano[1] · Yoshihiro Kashiba[1] · Akio Hirose[1]

Received: 16 June 2021 / Accepted: 30 September 2021 / Published online: 28 October 2021
© The Minerals, Metals & Materials Society 2021

Abstract

The reduction behavior of the surface oxide on Cu particles under a reducing gas atmosphere was investigated for a pressureless sinter joining. We conducted x-ray thermodiffraction analysis and simultaneous thermogravimetry, differential thermal analysis, and mass spectroscopy (TG–DTA–MS) under a reducing atmosphere to investigate the reduction and subsequent sintering behaviors of copper particles at different oxygen concentrations. The shear strength of the pressureless sinter joint decreased with increasing oxygen concentration. The thermodiffraction results revealed that the reduction onset of Cu_2O started at the same temperature (220°C), whereas the reaction markedly persisted at higher oxygen concentrations. Cu sintering progressed significantly after the reduction due to generation of Cu nanoparticles. The TG–DTA–MS results indicated that H_2O formation temperature associated with the reduction depends on the oxygen concentration, consistent with the thermodiffraction results. The surface oxides were found to play an important role in pressureless sinter joining via nanoparticle formation, while the presence of a large amount of oxide delayed the reduction and subsequent sintering.

Keywords Nanoparticles · reduction behavior · copper · copper oxide · pressureless sintering

Introduction

The high sinterability and thermostability of metal nanoparticles facilitate the implementation of the sinter joining process for the fabrication of power devices.[1–4] Nanoparticles exhibit low-temperature sinterability because of an apparent melting point depression,[5,6] which is attributed to their high surface-to-volume ratio.[7,8] Nanoscale sintering processes have been studied using nanoparticles and in situ-generated nanoparticles derived from metal precursors for Ag and Cu [[9–12] (silver oxide, Cu oxide)[13,14] (Ag salt)]. In particular, in situ-generated nanoparticles can help obtain a superior joint between materials and substrates. Hirose et al. reported in situ production of Ag nanoparticles during the joining process for metal substrates using a mixture of Ag_2O and a reducing solvent,[9] which led to the development of metallization-free direct joining of semiconductor materials and ceramics[15–18] and the utilization of Cu oxide particles.[10,11] Furthermore, the sintering behavior owing to nanoparticle generation facilitated the use of metal precursors and metal particles as starting materials; Ag nanoparticles can be generated during heating in the joining process using Ag microparticles, which promotes the sintering of Ag particles.[19,20]

The sintering of microscale Cu particles is generally more difficult than Ag sintering although Cu has desirable characteristics, such as thermostability, low migration, and electrical conductivity, allowing the successful joining[21] and writing processes for the fabrication of printed electronics. Therefore, Cu nanoparticles are typically considered for joining and related processes.[22,23] In contrast, the temporary oxidation on the surface of Cu particles and the subsequent reduction by a reducing atmosphere involving hydrogen or formic acid can facilitate the joining of microscale Cu particles.[24–26] The bonding process through the oxidation–reduction reaction results from the formation of Cu_2O nanoparticles during the oxidation and subsequent formation of Cu

✉ Tomoki Matsuda
t-matsu@mapse.eng.osaka-u.ac.jp

[1] Division of Materials and Manufacturing Science, Graduate School of Engineering, Osaka University, 2-1 Yamadaoka, Suita 565-0871, Japan

[2] JX Nippon Mining and Metals Corporation, Hitachi, Ibaraki 317-0056, Japan

[3] Rigaku Corporation, 3-9-12, Matsubara-cho, Akishima-shi, Tokyo 196-8666, Japan

nanoparticles, which is similar to the reduction process of Cu oxide particles reported by Yao et al.[10]

As it is important to induce the reduction of the oxidized layer in this type of joining process, the initially surface-oxidized Cu particles are expected to be ideal joining material candidates. A reducing atmosphere, such as H_2, including forming gas and formic acid, can support the sintering of Cu particles at elevated temperatures by inducing the reduction of Cu oxide,[26,27] thus realizing pressureless or low-pressure sinter joining. We demonstrated pressureless sinter joining under a forming gas atmosphere using surface-oxidized Cu particles. It was found that the sintering of Cu particles can be promoted by the in situ-generated Cu nanoparticles derived from oxides, similar to the bonding via the oxidation–reduction process. However, the mechanism of and conditions for the initial oxidation of Cu particles suitable for the joining process have not been extensively investigated. Evaluating the reduction behavior of the initially oxidized Cu particles can contribute to the design of joining materials and processes. In this study, we investigated the reduction behavior of initially oxidized Cu particles in terms of its influence on the bonding ability in pressureless sinter joining by performing in situ thermodiffraction and thermal analyses under a reducing atmosphere.

Experimental Details

Three types of Cu particles with diameters D_{50} of 0.53 μm (A), 0.61 μm (B), and 0.95 μm (C) were prepared for joining a material through oxidation in an alkaline solution under various treatment times of (A) 1 h, (B) 12 h, and (C) 48 h. The diameter of particles was measured by laser diffraction particle sizing (Malvern Panalytical, Mastersizer 3000). The carbon and oxygen concentrations in submicron copper particles after alkaline treatment were measured to be 0.46%C and 1.1%O for Cu particles-A, 0.6%C and 1.3%O for Cu particles-B, and 0.73%C and 2.5%O for Cu particles-C, which were analyzed by the infrared absorption method (LECO, TC600). Figure 1 shows the field-emission scanning electron microscopy (FE-SEM; Hitachi, S-4800), transmission electron microscopy and dark-field scanning transmission electron microscopy (TEM/STEM; Thermo Fisher Scientific, Talos F200i) images of Cu particles-A–C, wherein the oxide layer present on the Cu particles becomes thick depending on the alkaline solution treatment. Fast Fourier transform (FFT) images shown in Fig. 1e represent Cu_2O on the surface of Cu particles. Moreover, STEM images show that the oxide layer thickness of Cu particles-A (Fig. 1d) was on the order of several nanometers and that of Cu particles-C (Fig. 1f) was >10 nm. Small particles were formed and

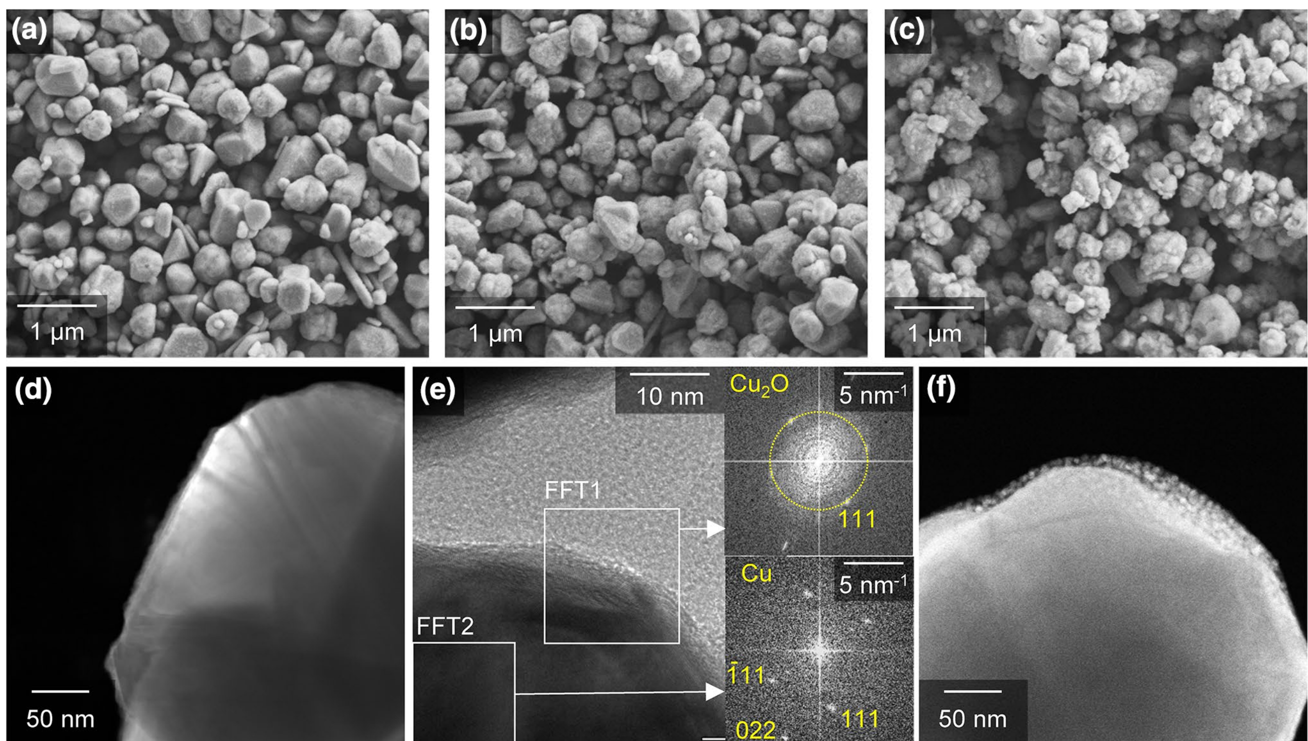

Fig. 1 FE-SEM and DF-STEM/TEM images of Cu particles (a), (d, e) A, (b) B, and (c), (f) C used for joining materials. FFT images in (e) show the presence of Cu_2O on the surface of Cu.

aggregated on the surface of the Cu particles for longer alkaline treatment times, which led to an increase in the median diameter. Submicron Cu particle pastes (samples A–C) were prepared by mixing Cu particles-A–C with dihydroterpineol and thermoplastic resin after surface treatment using a nonionic surfactant.

For the pressureless sinter joining experiments, bare Cu discs (5 (φ) × 2 mm (t) and 10 (φ) × 5 mm (t)) were used as the joining specimens. These specimens were subjected to 10 min of ultrasonic cleaning in an acetone bath prior to joining. Pastes A–C were applied to a thickness of 50 μm on the lower Cu disc and preheated in an atmospheric furnace to evaporate any excess organic solvent. The joining experiments were performed under N_2–3%H_2 (forming gas) atmospheric conditions using a vacuum reflow solder system (UNITEM, RSS-350-210); the joining specimen was heated after vacuuming at room temperature. The temperature rise rate, joining temperature, and holding time were 60°C/min, 300°C, and 30 min, respectively. Subsequently, the sample was cooled under forced air. The joint strength was measured as the average value of three joints by conducting shear tests at a crosshead speed of 0.5 mm/s.

FE-SEM observations were performed on samples A–C to investigate the microstructural changes in the Cu particles with the oxygen concentration through heating under N_2–3%H_2 atmospheric conditions. Further, X-ray thermodiffraction analysis under He–4%H_2 and simultaneous thermogravimetry, differential thermal analysis, and mass spectroscopy (TG–DTA–MS) measurements under N_2–3%H_2 were performed to evaluate the crystal structure changes during the reduction behavior of Cu particles and the corresponding thermal change in the paste, respectively. X-ray diffraction (XRD) measurement under elevated temperature (thermodiffraction analysis) was performed using a Reactor X system equipped in SmartLab (Rigaku) at a heating rate of 10°C/min from room temperature to 350°C under a He–4%H_2 atmosphere.[28] XRD analysis was performed in reflection geometry under point-focused radiation of Cu Kα (1.5406 Å) using a 2D detector (Rigaku SmartLab with HyPix-3000). TG–DTA (Rigaku, Thermo plus TG8120) combined with quadrupole mass spectrometry (Canon Anelva, M-100QA-M) was performed at a heating rate of 60°C/min from room temperature to 350°C under a N_2–3%H_2 atmosphere.

Results and Discussion

Figure 2a shows the results of shear tensile tests for the joint bonded using submicron Cu particles with the oxide concentration in the range of 1.2–3.8%. Although Cu particles with a thin oxide layer showed a high joint strength above 20 MPa, the joint strength decreased with an increase in the oxide layer thickness. Figure 2b–d shows the FE-SEM images of the sintering particles at 250°C and 300°C for 30 min. Nanoparticles were formed on the surface of low-oxygen submicron copper particles even at 250°C (Fig. 2b), and the sintering and necking of the Cu particles progressed at 300°C (Fig. 2c). In contrast, the sintering did not progress as markedly even at 300°C under higher oxygen concentrations (Fig. 2d, e). Notably, some of the nanoparticles were not sintered (Fig. 2d, e) and an oxide layer was formed on the high-concentration oxygen particles (Fig. 2e). As Cu particles without an oxide layer has difficulty in yielding a joint[29], the in situ formation of Cu nanoparticles is believed to have supported the sintering of submicron Cu particles for pressureless joining, similar to that in Ag nano-sintering. Furthermore, these results indicate that pressureless sintering and subsequent joining behaviors are significantly influenced by the reduction behavior of the copper oxide layer. To clarify the influence of the reduction behavior of the oxide layer on the sintering and joining processes under the N_2–H_2 atmosphere, we performed XRD and TG–DTA–MS measurements under the identical N_2–H_2 atmosphere.

Figure 3 shows the thermodiffraction data for each sample upon heating under the He–4%H_2 atmosphere, where Fig. 3a shows the raw data obtained from the 2D detector. Figure 3b shows the relationship between the temperature dependence of the diffraction profile calculated from the raw 2D diffraction results. The diffraction peak at approximately 47° corresponds to the (111) plane of Al, which was used as the sample mount jig. As each paste showed Cu (111) and (200) peaks and Cu_2O (111) and (200) peaks at room temperature before heating, Cu_2O was present on the copper particles, as shown in Fig. 2. Cu_2O peaks disappeared at approximately 250°C during heating, revealing the reduction of Cu_2O owing to the He–4%H_2 atmosphere. Although it has been reported that the reduction of Cu_2O particles occurs at approximately 300°C under the H_2 atmosphere[27] and glycol solvent[10], the thin oxide layer under the He–4%H_2 atmosphere can be reduced at lower temperatures. The Cu_2O (111) and Cu (200) peaks were analyzed to compare the reduction of Cu_2O and the sintering behavior of Cu for each paste.

Figure 3c–f show the analyzed data for the Cu_2O (111) and Cu (200) peaks during heating for each submicron copper paste. The temperature-dependent evolution of the normalized intensity for Cu_2O (111) shows that Cu_2O disappears at higher temperatures under a high oxygen concentration: 300°C for sample A to 350°C for sample C. On the other hand, there is little difference in the onset temperature of reduction at 220°C (Fig. 3c). To evaluate the Cu (200) peak, the diffraction angle, full width at half maximum (FWHM), and area intensity were estimated by fitting the diffraction profile using the Voigt function to compare the microstructural evolution of Cu; the diffraction angle was converted to d-spacing using Bragg's law. As shown in Fig. 3d–f, the d-spacing value generally increases with

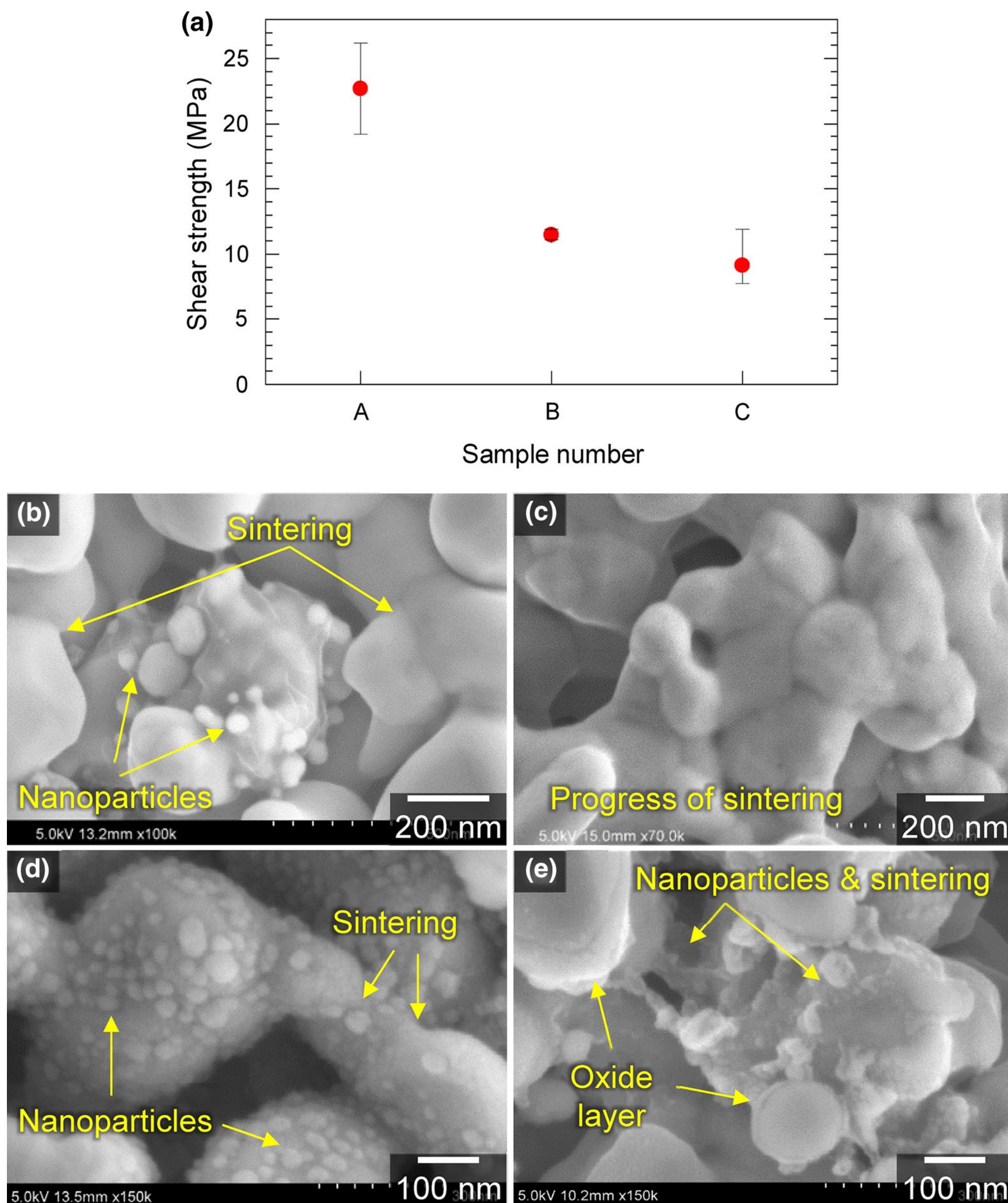

Fig. 2 Pressureless sinter joining results using submicron copper paste in N_2–H_2 atmosphere. (a) Shear strength of copper joints using each copper particle with different oxygen concentrations. FE-SEM images of the sintering behavior of copper particles after holding for 30 min at (b) 250°C for sample A and 300°C for (c) sample A, (d) sample B, and (e) sample C.

increasing temperature owing to the expansion of the lattice during heating. Furthermore, FWHM, which is related to the crystallite size as expressed by Scherrer's equation[30], gradually decreases with increasing temperature owing to the progress of crystallization or particle sintering. However, the gradient of *d*-spacing and FWHM temporarily decreased above 200°C. At this time, the area intensity reached its maximum value. The onset temperature for the increase in the intensity was approximately consistent with that of Cu_2O reduction, as shown in Fig. 3c. These results indicate that the reduction of Cu_2O generates new copper nanoparticles. The diffraction profile was due to the sum of the existing copper particles, and the gradient of the *d*-spacing should be changed. Furthermore, the high rate of decrease in the FWHM can be attributed to the progress of Cu particle sintering driven by the reduction of Cu_2O for the following reasons: (i) formation of Cu nanoparticles, which assists the sintering of submicron Cu particles as a bridging effect, and (ii) full exposure of the submicron copper surface.

Figure 4 shows the simultaneous TG–DTA–MS analyses under a N_2–H_2 atmosphere for submicron copper paste. The TG results show a major weight decrease up to 150°C and

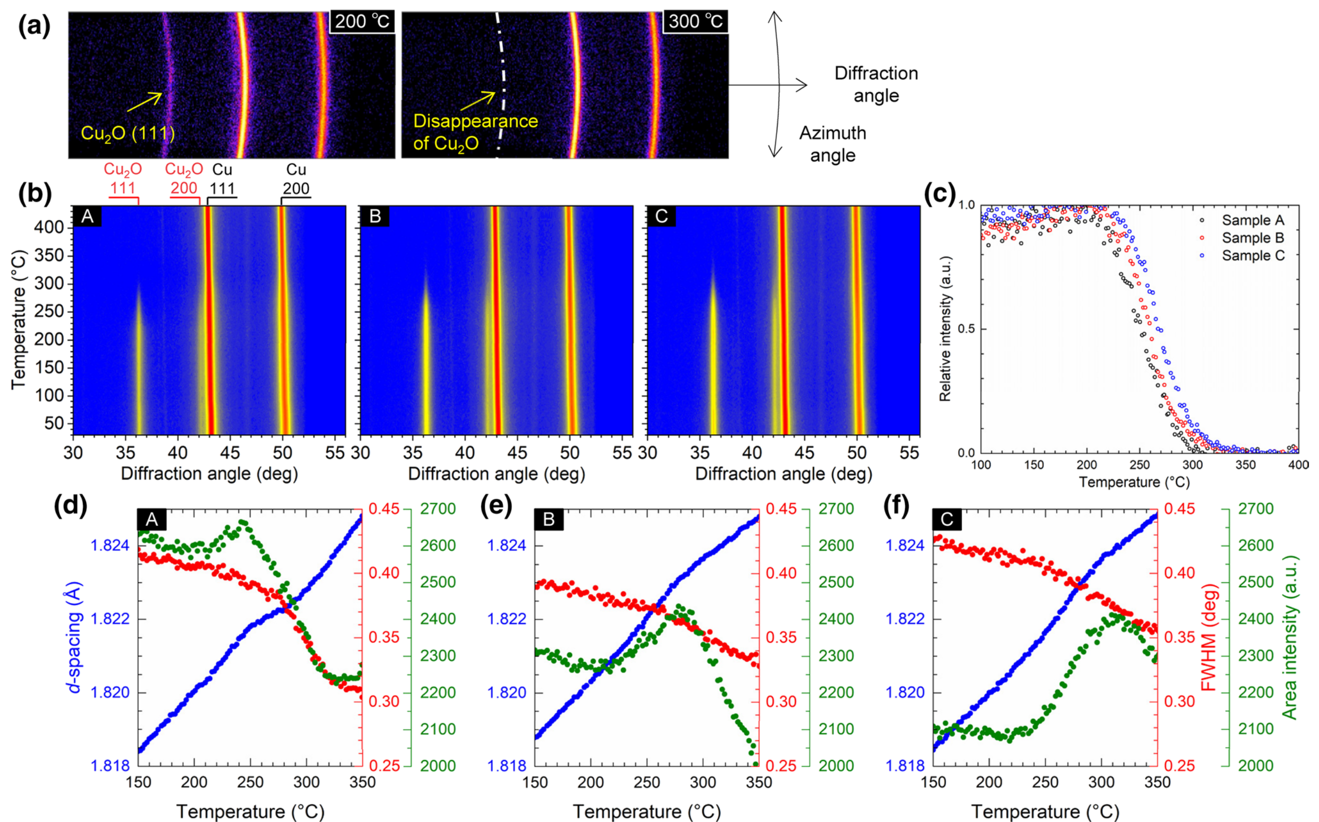

Fig. 3 Thermodiffraction measurement for samples A–C heated from room temperature to 450°C under He–3%H_2 reduction atmosphere. (a) Representative result of the 2D detector obtained at 200 and 300°C. (b) Diffraction intensity change dependence on the elevated temperature. (c) Change in the relative intensity of Cu_2O (111) normalized by the intensity at approximately 200°C. Variations in the *d*-spacing, FWHM, and area intensity of the Cu (200) profile fitted by the Voigt function for (d–f) samples A–C.

a subsequent minor weight decrease from 200°C to 300°C for every paste (Fig. 4a). An endothermic reaction occurs at approximately 120°C, in accordance with the weight decrease (Fig. 4b), whereas there is little change in the MS measurement for H_2O ($m/z = 18$) and CO_2 ($m/z = 44$) (Fig. 4c). These results indicate that the weight decrease at 100°C corresponds to the evaporation of the organic solvent (i.e., dihydroterpineol), which does not involve redox or decomposition reactions.

On the other hand, exothermic reactions occurred in accordance with the weight decrease above 200°C. Furthermore, the MS results showed an increase in CO_2 and subsequent H_2O above 200°C. There was correspondence regarding (i) weight decrease, first exothermic reaction, and increase in CO_2 MS, and the subsequent (ii) second exothermic reaction and increase in H_2O MS. Furthermore, both the combustion of the organic protective layer on the copper particles and the reduction of the copper oxide caused the exothermic reaction[10], involving the generation of CO_2 in the combustion and of H_2O in the general reduction process as follows: $Cu_2O + H_2 \rightarrow 2Cu + H_2O$. Therefore, it is supposed that submicron copper paste undergoes (a) evaporation of dihydroterpineol as a paste material, (b) combustion of the organic protective layer, and (c) reduction of the copper oxide layer. Based on the results obtained for samples A–C, the behaviors above 200°C changed with the oxygen concentration. The submicron copper particles with low oxygen concentration resulted in earlier behaviors, particularly in terms of the reduction of copper oxide with the generation of H_2O, than that under higher oxygen concentrations, which is consistent with the Cu_2O annihilation and Cu generation behaviors observed in the thermodiffraction measurements (Fig. 3). This hypothesis is in good agreement with the report by LaGrow et al., which confirmed that the reduction of Cu_2O to Cu occurs preferentially at Cu/Cu2O interface[31].

As expected, it is considered that the surface oxide contributes to pressureless sinter joining via the generation of Cu nanoparticles, which promotes the sintering of the initial particles owing to the bridging effect.[16,19] In contrast, the excess oxide conversely delays the sinter joining in the N_2–3%H_2 atmosphere because the reduction cannot be completed at low temperatures or short holding times, because of which the oxide remains and disturbs the sintering of the Cu particles. This is consistent with the results obtained by Kim

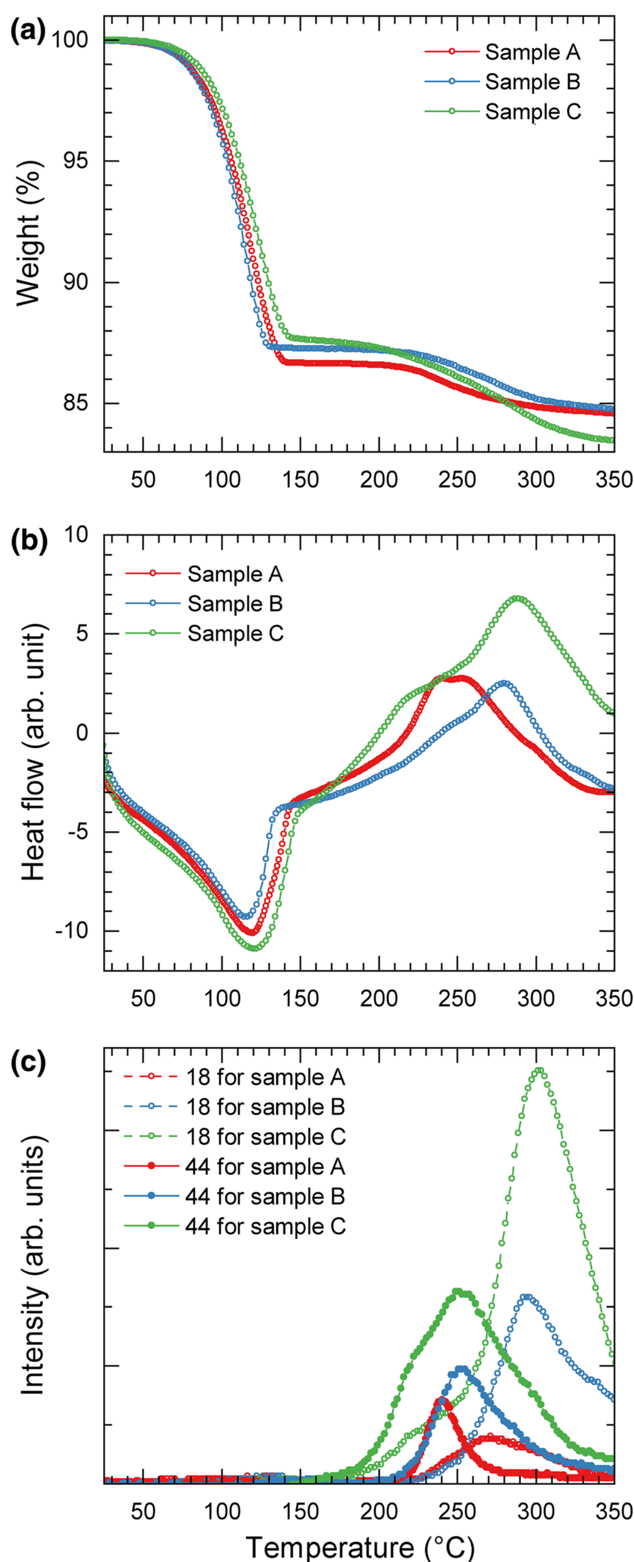

Fig. 4 Simultaneous TG–DTA–MS results for samples A–C under N_2–3%H_2 atmosphere: (a) TG curves. (b) DTA curves. (c) MS curves for m/z = 18 and *m*/*z* = 44.

et al., where Cu_2O powder starts to reduce at 300°C with an elevated temperature rate of 20°C/min under He–5%H_2 flow,[27] which indicates that the full reduction of Cu_2O particles requires a higher temperature or a longer holding time. Therefore, the appropriate design of surface oxides relevant to the reducing atmosphere, such as the concentration and reducing ability of the substance, plays a significant role in pressureless sinter joining using submicron copper particles.

Conclusions

In summary, we investigated the reduction behavior of surface oxide on submicron Cu particles in the pressureless sinter joining of a bare Cu substrate under a reducing gas atmosphere. Thermodiffraction and TG–DTA–MS analyses under a reducing atmosphere were performed to study copper particles with different oxygen concentrations. The shear strength results showed a decreasing strength with increasing oxygen content. Thermodiffraction results revealed that the reduction reaction persists in Cu particles with higher oxygen concentrations, whereas the onset of the reduction of Cu_2O starts at the same temperature of approximately 220°C. The FWHM of Cu diffraction accelerated with a temporal delay of increasing lattice constant after the initial reduction behavior, which indicated that Cu sintering markedly progresses after the onset of reduction, attributed to Cu nanoparticle generation. Furthermore, TG–DTA–MS results showed that the temperature for H_2O formation associated with the reduction depends on the oxygen concentration, in accordance with the thermodiffraction results. The surface oxide contributes to pressureless sinter joining via the generation of Cu nanoparticles, while the large amount of oxide formed delays the reduction and subsequent sintering.

Conflict of interest The authors declare that they have no known competing financial interests or personal relationships that could have appeared to influence the work reported in this paper.

References

1. J.G. Bai, J. Yin, Z. Zhang, G.Q. Lu, and J.D. Wyk, High-temperature operation of SiC power devices by low-temperature sintered silver die-attachment. *IEEE Trans. Adv. Packag.* 30, 506 (2007).
2. T. Youssef, W. Rmili, E. Woirgard, S. Azzopardi, N. Vivet, D. Martineau, R. Meuret, G. Le Quilliec, and C. Richard, Power modules die attach: a comprehensive evolution of the nanosilver sintering physical properties versus its porosity. *Microelectron. Relib.* 55, 1997 (2015).
3. S.A. Paknejad, and S.H. Mannan, Review of silver nanoparticle based die attach materials for high power/temperature applications. *Microelectron. Relib.* 70, 1 (2017).
4. H. Zhang, C. Chen, J. Jiu, S. Nagao, and K. Suganuma, High-temperature reliability of low-temperature and pressureless micron Ag

sintered joints for die attachment in high-power device. *J. Mater. Sci.: Mater. Electron.* 29, 8854 (2018).
5. A.N. Goldstein, C.M. Echer, and A.P. Alivisatos, Melting in semiconductor nanocrystals. *Science* 256, 1425 (1992).
6. S.L. Lai, J.Y. Guo, V. Petrova, G. Ramanath, and L.H. Allen, Size-dependent melting properties of small tin particles: nanocalorimetric measurements. *Phys. Rev. Lett.* 77, 99 (1996).
7. K.J. Klabunde, J. Stark, O. Koper, C. Mohs, D.G. Park, S. Decker, Y. Jiang, I. Lagadic, and D. Zhang, Nanocrystals as stoichiometric reagents with unique surface chemistry. *J. Phys. Chem.* 100, 12142 (1996).
8. P. Peng, A. Hu, A.P. Gerlich, G. Zou, L. Liu, and Y.N. Zhou, Joining of silver nanomaterials at low temperatures: processes, properties, and applications. *ACS Appl. Mater. Interfaces* 7, 12597 (2015).
9. A. Hirose, H. Tatsumi, N. Takeda, Y. Akada, T. Ogura, E. Ide, and T. Morita, A novel metal-to-metal bonding process through in-situ formation of Ag nanoparticles using Ag2O microparticles. *J. Phys. Conf. Ser.* 165, 012074 (2009).
10. T. Yao, T. Matsuda, T. Sano, C. Morikawa, A. Ohbuchi, H. Yashiro, and A. Hirose, In-situ study of reduction process of CuO paste and its effect on bondability of Cu-to-Cu joints. *J. Electron. Mater.* 47, 2193 (2018).
11. F. Paglia, D. Vak, J. van Embden, A.S.R. Chesman, A. Martucci, J.J. Jasieniak, and E.D. Gaspera, Photonic sintering of copper through the controlled reduction of printed CuO nanocrystals. *ACS Appl. Mater. Int.* 7, 25473 (2015).
12. Y. Zuo, S. Carter-Searjeant, M. Green, L. Mills, and S.H. Mannan, Low temperature Cu joining by in situ reduction-sintering of CuO nanoparticle for high power electronics. *Adv. Powder Technol.* 31, 4135 (2020).
13. S. Hausner, P. Frenzel, J. Noll, G. Wagner, and H. Lang, Joining of copper at low temperatures using silver(I) carboxylates. *Weld. World* 62, 1215 (2018).
14. L. Tang, G. Gan, X. Yu, C. Liu, and J. Cheng, Study on the mechanism of forming silver nanoparticles on micronscale flake silver powder. *Mater. Res. Exp.* 7, 105001 (2020).
15. K. Asama, T. Matsuda, T. Ogura, T. Sano, M. Takahashi, and A. Hirose, Low-temperature metal-to-alumina direct bonding process utilizing redox reaction between silver oxide and organic agent. *Mater. Sci. Eng. A* 702, 398 (2017).
16. T. Matsuda, K. Inami, K. Motoyama, T. Sano, and A. Hirose, Silver oxide decomposition mediated direct bonding of silicon-based materials. *Sci. Rep.* 8, 10472 (2018).
17. K. Motoyama, T. Matsuda, T. Sano, and A. Hirose, AlN-to-metal direct bonding process utilizing sintering of Ag nanoparticles derived from the reduction of Ag2O. *J. Electron. Mater.* 47, 5780 (2018).
18. T. Matsuda, S. Yamada, A. Takeuchi, K. Uesugi, M. Yasutake, T. Sano, M. Ohata, and A. Hirose, Fracture behavior of thermally aged Ag–Cu composite sinter joint through microscale tensile test coupled with nano X-ray computed tomography. *Mater. Des.* 206, 109818 (2021).
19. H. Zhang, Y. Gao, J. Jiu, and K. Suganuma, In situ bridging effect of Ag2O on pressureless and low-temperature sintering of micron-scale silver paste. *J. Alloy. Compd.* 696, 123 (2017).
20. C. Chen, and K. Suganuma, Large-scale ceramic–metal joining by nano-grained Ag particles paste sintering in low-temperature pressure-less conditions. *Scr. Mater.* 195, 113747 (2021).
21. T.F. Chen, and K.S. Siow, Comparing the mechanical and thermal-electrical properties of sintered copper (Cu) and sintered silver (Ag) joints. *J. Alloy Compd.* 866, 158783 (2021).
22. J. Kwon, H. Cho, Y.D. Suh, J. Lee, H. Lee, J. Jug, D. Kim, D. Lee, S. Hong, and S.H. Ko, Flexible and transparent Cu electronics by low-temperature acid-assisted laser processing of Cu nanoparticles. *Adv. Mater. Technol.* 2, 1600222 (2017).
23. M. Kanzaki, Y. Kawaguchi, and H. Kawasaki, Fabrication of conductive copper films on flexible polymer substrates by low-temperature sintering of composite Cu ink in air. *ACS Appl. Mater. Interfaces* 9, 20852 (2017).
24. R. Gao, S. He, Y.-A. Shen, and H. Nishikawa, Effect of substrates on fracture mechanism and process optimization of oxidation-reduction bonding with copper microparticles. *J. Electron. Mater.* 48, 2263 (2019).
25. R. Gao, S. He, J. Li, Y.-A. Shen, and H. Nishikawa, Interfacial transformation of preoxidized Cu microparticles in a formic-acid atmosphere for pressureless Cu-Cu bonding. *J. Mater.: Sci. Mater. Electron.* 31, 14635 (2020).
26. T. Yonezawa, H. Tsukamoto, and M. Matsubara, Low-temperature nanoredox two-step sintering of gelatin nanoskin-stabilized submicrometer-sized copper fine particles for preparing highly conductive layers. *RSC Adv.* 5, 61290 (2015).
27. J.Y. Kim, J.A. Rodriguez, J.C. Hanson, A.I. Frenkel, and P.L. Lee, Reduction of CuO and Cu2O with H2: H embedding and kinetic effects in the formation of suboxides. *J. Am. Chem. Soc.* 125, 10684 (2003).
28. R. Kawai, H. Yukawa, A. Suzuki, T. Nambu, and Y. Murata, Alloying effects of Fe and Al on formation and decomposition temperatures of vanadium hydride, V2H. *Int. J. Hydro. Energy* 42, 22564 (2017).
29. X. Liu, and H. Nishikawa, Low-pressure Cu-Cu bonding using in-situ surface-modified microscale Cu particles for power device packaging. *Scr. Mater.* 120, 80 (2016).
30. B.D. Cullity, S.R. Stock, Elements of X-Ray Diffraction, 3rd edn. (Prentice-Hall 2001).
31. A. LaGrow, M. Ward, D. Lloyd, P. Gai, and E.D. Boyes, Visualizing the Cu/Cu2O interface transition in nanoparticles with environmental scanning transmission electron microscopy. *J. Am. Chem. Soc.* 139, 179 (2017).

Publisher's Note Springer Nature remains neutral with regard to jurisdictional claims in published maps and institutional affiliations.